1-1-2016

NIH Visible Human Project Humerus Numerical and Physical Models: Characterization for Osteogenesis Imperfecta Fracture Study

Prateek Grover
Department of Rehavilitation Medicine, Washington University, St. Louis, MO

Gerald F. Harris
Marquette University, gerald.harris@marquette.edu

Published version. *Transitional Care in Osteogenesis Imperfecta: Advances in biology, Technology, and Clinical Practice*, (2016): pp. 161-176. Publisher link.

10 NIH VISIBLE HUMAN PROJECT HUMERUS NUMERICAL AND PHYSICAL MODELS: CHARACTERIZATION FOR OSTEOGENESIS IMPERFECTA FRACTURE STUDY

Prateek Grover, M.D., Ph.D.[1]
Gerald Harris, Ph.D., P.E.[2,3]

[1] Department of Rehabilitation Medicine, Washington University, St. Louis, MO
[2] Orthopaedic and Rehabilitation Engineering Center (OREC),
Marquette University and The Medical College of Wisconsin, Milwaukee, WI
[3] Shriners Hospitals for Children, Chicago, IL

INTRODUCTION

Long bone fractures in the osteogenesis imperfecta (OI) population present with a bimodal age distribution, in the pre-adolescent and post–middle age groups.[1] The humerus is the most common upper extremity bone to fracture.[1] The fractures are most commonly transverse, subperiosteal, minimally displaced,[1] not prone to nonunion,[1] and often located at the convexity of the curved diaphysis.[2] The increased fracture risk has been attributed to multiple genetic mutations that result in quantitative (OI type I) and/or qualitative (OI types II-IV) changes in type I collagen.[3] Consequent alterations in bone material-properties and structure have been documented. The major cortical and cancellous bone material-properties affected include bone mineral density,[4,5] longitudinal modulus and hardness.[6,7] Alterations in structure at the microscopic level include thinning of trabeculae,[8] loss of cancellous and cortical bone volume,[9] loss of Haversian lamellar bone structure and resemblance to fetal woven bone[1] Structural alterations at the macroscopic level include a reduction in cross-sectional area as well as cortical width.[10,11]

Refracture at or close to the site of previous fracture is also well documented.[1] Proposed contributory factors for refracture include joint contractures and deformity of the upper extremities.[12] Humeral deformities are most common in the postero-medial (35.6%) and medial (32.2%) planes,

followed by the antero-medial plane (27.1%). Pure posterior (3.4%) and anterior (1.7%) deformities are much less common.[13] The greatest incidence of deformity has been attributed variably to both OI type I[1] and type III.[13] Amako further quantified the incidence of severity of humeral deformity in OI type III. Overall, the "no deformity" group was larger than any of the deformity groups. Among the "deformity" groups, the "30-59 degrees" was the largest group, followed by the "greater than 60 degrees" and "0-29 degree" groups.

In addition to humeral deformity, additional loads imposed on the humerus in the OI subpopulation ambulating with assistive devices such as Lofstrand crutches could further increase fracture risk.[14] This predisposition of the humerus to fracture and refracture in OI, as a consequence of altered material properties and geometry, as well as increased functional requirements (ambulatory aids) is presented in Figure 1, and can be studied at the macroscopic structural level using anatomic humerus models and corresponding 3D computational geometry.

The only known anatomic models of the human humerus are the Composite humerus models (3rd and 4th generation, Sawbones Worldwide, Pacific Research Labs, Vashon, WA). The 4th generation cortical and cancellous simulation materials in these models have been designed to closely simulate human bone material properties, including fracture toughness, fatigue life, strength, modulus and thermal stability.[15] Consistent geometry and small-range variability in material properties have allowed researchers to use similar femur and tibial models for clinical applications,[16,17] as an alternative to cadaveric bones, which require strict preservation and handling precautions.[18] However, increased fracture risk in the humerus in OI has not been studied using these models.

In addition, the 3D-computational geometry of these models lacks the potential for source-derived addition of muscle attachments, as would be possible for an anatomic model derived from a complete body visceral and musculoskeletal image dataset, such as the NIH Visible Human Project.[19] This presently non-extant muscle attachment-mapped geometry of the humerus, analogous to the existing "Standardized 3D computational geometry" of the composite femur,[20] has benchmark value.

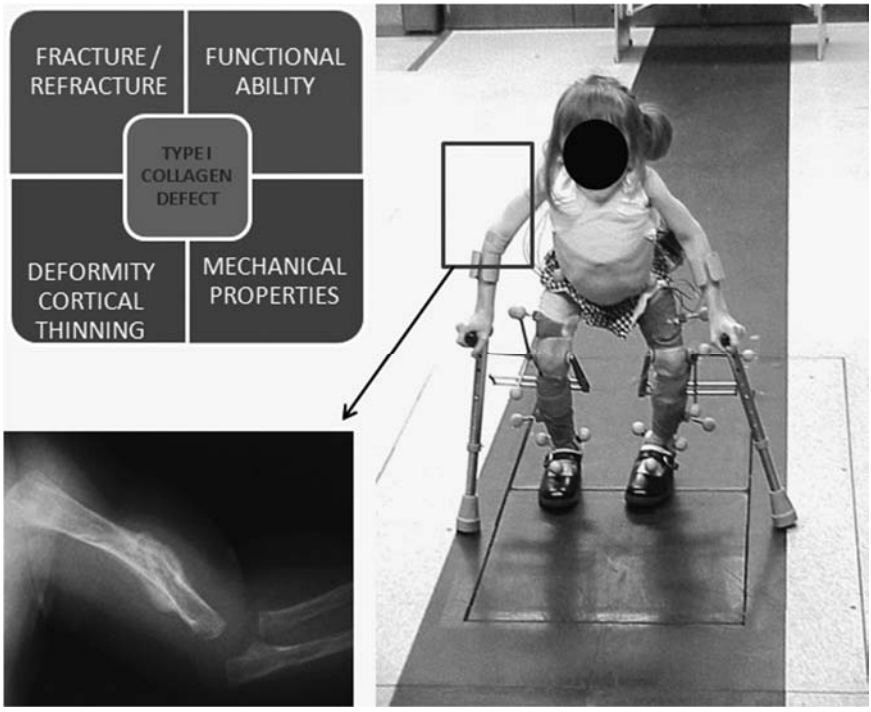

Figure 1. Factors predisposing the humerus to fracture and refracture in osteogenesis imperfecta.

Finally, the NIH Visible Human Project (NIH VHP) image-dataset based anatomic humerus physical model and its corresponding 3D-computational geometry can be used together as a "Reference Humerus" model to create a finite element (FE) humerus model. This FE model can be modified to simulate OI, and study both pathology-specific and patient-specific fracture risk. No standardized physical model and corresponding computational geometry for developing FE models of the humerus has been reported in the literature.

The goal of the overall project is to study humeral fracture risk in OI, especially in the subpopulation ambulating with Lofstrand crutches, using a mechanically and anatomically characterized "Reference Humerus" tool. The project is divided into three phases. The present study focuses on the first phase of this project, namely, the design and development of the a "Reference Humerus" model, comprising both a physical model and computational geometry, from the NIH Visible Human Project, based upon identified "definition-of-reference" criteria. Anatomic and mechanical

characterizations of this model, followed by the model's application to OI for studying fracture risk, comprise the second and third phases, respectively.

METHODS

"Definition-of-reference" criteria were identified and incorporated in the development process of the "Reference Humerus" model. The development process was comprised of three sequential phases, namely, (a) development of 3D-humerus geometry from the NIH Visible Human Project image dataset, (b) development of a physical model, the Humerus-Visible Human Project (H-VHP) from the 3D-humerus geometry, and (c) development of 3D-computational geometry of the H-VHP. The physical model, H-VHP, and its 3D-computational geometry together comprise the "Reference Humerus" model.

"Definition-of-Reference" Criteria

Five criteria were defined for the development of the "Reference Humerus" model. The first four criteria were used to accomplish the first phase of the project, which is the focus of this publication. The fifth criterion is pertinent to the second phase.

Physical Model, H-VHO: Standard Source of Geometry

The NIH Visible Human Project, comprised of MRI, CT, and new and old anatomical image subsets, has been used for a multitude of technical (image processing, virtual reality) and clinical (diagnosis, presurgical planning) research and teaching projects, as well as for commercial applications extending from art to industry, by approximately 2,000 licensees in over 48 countries.[19] As a source of geometry for an FE model of the humerus, the NIH VHP offers significant advantage over both composite humerus models [15] and cadaveric humeri. This is because this standard source of accurate, accessible, and complete musculoskeletal and visceral high-resolution anatomic data of one specific human enables potential addition of soft tissues such as muscles and ligaments, as well as joints to the osteoanatomy of the humerus. Among the data subsets, the new anatomic image subset is preferred to the CT scan subset, since the latter is lower in resolution and lacks complete definition of the distal humerus. A sample image slice from the NIH VHP newer anatomic image dataset demonstrating complete visceral and musculoskeletal image data is presented in Figure 2.

Figure 2. Sample image slice from the NIH VHP newer anatomic image dataset demonstrating complete visceral and musculoskeletal image data (distributed by National Technical Information Service, Springfield, VA 22161).

Standard Physical Model, H-VHP: Standard Development Protocol

Standard image segmentation techniques and software (Image J[21] and Mimics, M**aterialise US,** 44650 Helm Court, Plymouth, MI 48170, USA) were first identified from literature as part of the design process to create a 3D-humerus geometry from the Visible Human Project image dataset. The development criteria required identification of a standard manufacturer of long bone models, modification of the 3D-humerus geometry as per the physical model (H-VHP) manufacture requirements, and consensus on the minimum acceptable standards for the rapid prototyping manufacturing process.

Physical Model, H-VHP: Standard Materials of Manufacture

State-of-the-art cortex-simulation and cancellous-simulation materials were chosen to manufacture the physical (H-VHP) model. The cortex-simulation material is comprised of short-fiber reinforced epoxy, and the cancellous-simulation material is made of rigid polyurethane foam. Manufacturer documented properties for the 4th generation cortex-simulation material include longitudinal and transverse tensile moduli of 16.0 and 10.0 GPa, respectively, a compressive longitudinal modulus of 16.7 GPa, and material density of 1.64 gm/cc. Cancellous- simulation material properties include a modulus of 0.155 GPa, and density of 0.27 gm/cc.[15]

Standard 3D-Computational Geometry of H-VHP: Development Criteria

A standardized protocol involving sequential image processing (Mimics, Materialise US, Plymouth, MI 48170, USA), computer aided design (Solidworks, Dassault Systèmes SolidWorks Corporation, Waltham, MA 02451), and finite element techniques (Abaqus, Simulia, Rising Sun Mills,

Providence, RI, USA) was developed to derive the 3D-computational geometry from the physical model, H-VHP.

Reference Humerus: Clinical and Research Applicability Criteria

Protocols for the second phase of the project, namely, mechanical characterization of the physical model, H-VHP, and anatomic characterization of the corresponding 3D-computational geometry, were defined in accordance with this criterion. The protocol for mechanical characterization was guided by studies on experimental evaluation of mechanical properties of other composite and cadaveric humeri.[22] The anatomic characterization protocol was defined with reference to literature on surgical procedures and shoulder and elbow arthroplasty implant design.[23,24] Figure 3 presents some of the surgical anatomic parameters of the humerus that were identified.

"Reference Humerus" Model Development

Development of 3D-Humerus Geometry from the Visible Human Project Image Dataset

Cross-sectional anatomic image slices from the Visible Human Project Male Thorax image dataset were imported into Image J for preliminary evaluation. For the purpose of further importing these slices into Mimics, the image slices were converted into a stack of .bmp format images using the Batch Converter tool in Image J. However, preliminary examination of the dataset revealed three misaligned slices. To accurately realign these image slices using the StackReg tool in Image J, the .bmp data stack was converted into three .tiff data stacks, with an overlap of one image for each consecutive set. The three .tiff stacks were then realigned using the StackReg tool, and were converted back into one accurately aligned .bmp format stack. However, owing to the large image data size (9.7 MB/ image) as well as limitations on the size of imported stacks in Mimics, the data had to be imported from Image J into Mimics as three contiguous .bmp subset image stacks.

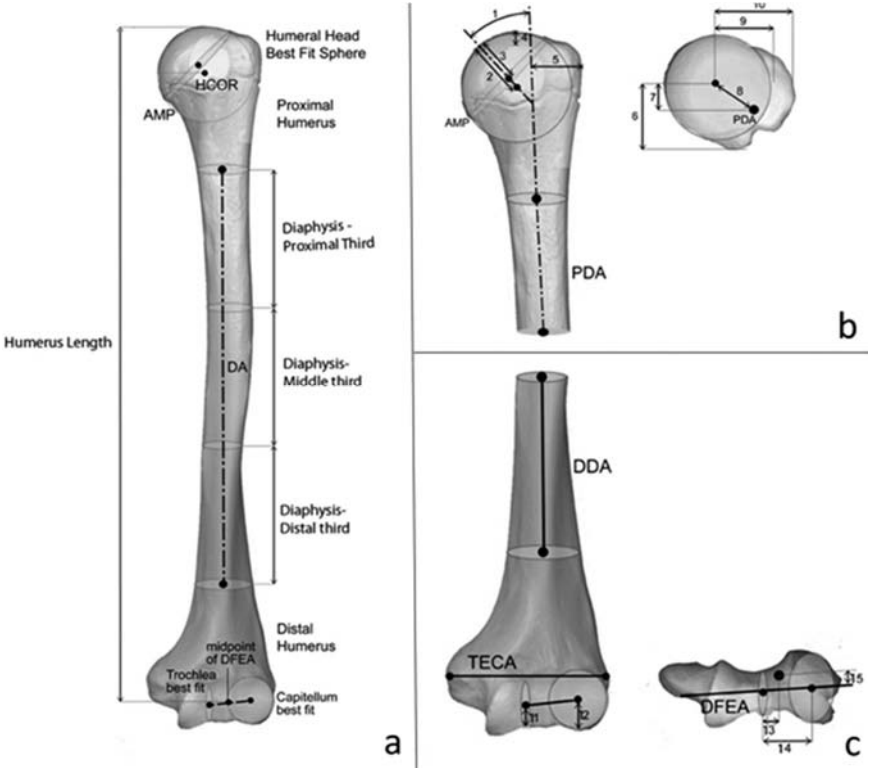

Figure 3. Surgical anatomic parameters of the humerus identified from the literature on shoulder and elbow arthroplasty for future anatomic characterization of the "Reference-Humerus" model. A. Humerus anatomic best-fits; b. Proximal humerus parameters; c. Distal humerus parameters. Parameters Illustrated: 1. Inclination; 2. Proximal Articular Surface radius; 3. Humeral Head height; 4.Humeral Head to Greater Tuberosity height; 5.Greater Tuberosity width; 6. Lesser Tuberosity — Anterior Offset; 7.Humeral Head — Posterior Offset; 8.Humeral Head — Total Offset; 9.Humeral Head — Medial Offset; 10.Greater tuberosity — Lateral Offset; 11.Trochlear Sulcus — Radius of Curvature; 12. Capitellum — Radius of Curvature; 13.Distal Flexion Extension Axis — Medial Offset; 14. Distal Flexion Extension Axis length; 15. Distal Flexion Extension Axis —Anterior Offset.

Mimics 9.0 was then used to window, threshold and segment the cross-sectional image slices within the stacks to include a smaller image area surrounding the humerus, and thus reduce the overall data size of each stack. The resulting three smaller sized stacks were combined into one, and reprocessed with windowing and thresholding to segment out the *outer cortex*, *inner cortex/outer cancellous* and *inner cancellous surfaces*. The three fine triangular geometric mesh surfaces were refined further and exported in .stl format.

Development of Physical Model, H-VHP from 3D-Humerus Geometry

The *outer cortex* and *inner cortex/outer cancellous surface* geometries (.stl format) were sent to a standard manufacturer of composite bones, Sawbones Worldwide (Pacific Research Labs, Vashon, WA, USA). Based upon these two .stl files, stereolithography files were generated, which were used to create individual molds for the cortex and the core, respectively, using the rapid prototyping technique. Additional manufacturing requirements necessitated the use of two transverse cross-pins, one each in the proximal and distal segments of the humerus, and a mandrel that spanned approximately the proximal three-fourths of the length of the model and exited at the proximal end.

The initial step in the model manufacturing process from the molds required the placement of the mandrel and crosspins into the core mold. The cavity of the core mold was filled with solid polyurethane foam cancellous-simulation material to encapsulate the mandrel and cross-pins. The core was then transferred to the cortex mold, where it was suspended in place by the mandrel and the cross-pins. Short-glass fiber reinforced epoxy cortex-simulation material was then injected around the core. Following heat-curing, the mandrel and cross-pins were removed, the model was cooled down, and the parting line of the model was trimmed. The model was then heat post-cured and modified to regain the original anatomic configuration.

Development of 3D-Computational Geometry of the H-VHP

The physical model was scanned into 320 transverse sections using a CT scanner, at a resolution of 512 x 512 x 320 pixels, with a voxel size of 0.3mm x 0.3mm x 1.25mm at 8 bits. The transverse images were imported into Mimics, and mutually exclusive 3D *cortical, cancellous and medullary surfaces* of the H-VHP physical model were developed and exported as .stl files. To convert the .stl files into a usable format for ABAQUS, the .stl geometric mesh surface files (comprised of triangles) were imported into Solidworks.

Using the Scan-to-3D tool in Solidworks, the triangle mesh surfaces were then converted into polygon geometric mesh surfaces, since the polygons better approximated the curved osteoanatomy of the humerus, compared with triangles. The polygon geometry mesh surfaces were then imported into ABAQUS as three volumes. These three volumes, namely, the *cortical volume,* the *cancellous volume,* and the *medullary canal volume* were merged, while

retaining intersecting surfaces to ensure that consecutive volumes shared adjacent surfaces but did not overlap (Figure 4).

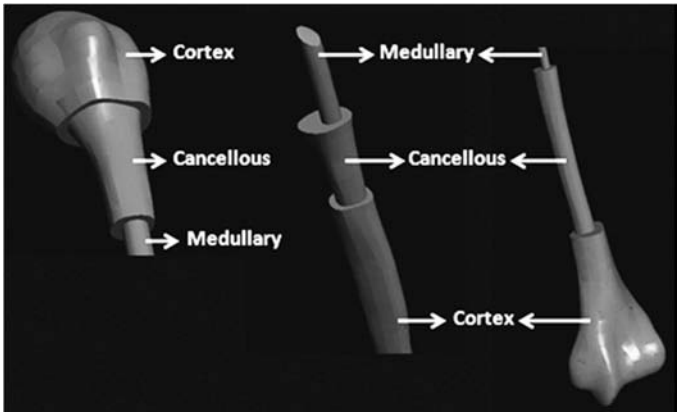

Figure 4. 3D-computational geometry of H-VHP: Cortical, cancellous and medullary canal volumes, with retained intersecting surfaces.

RESULTS

3D Humerus Geometry Developed from the NIH Visible Human Project Image Dataset

The 3D-humerus geometry developed from the NIH Visible Human Project image dataset included three non-intersecting geometric mesh surfaces, namely, the *outer cortex, inner cortex/outer cancellous and inner cancellous surfaces*. Each mesh surface was composed of thousands of very small triangles that helped to closely approximate the curved surfaces in the humerus osteoanatomy. Anterior, posterior, lateral oblique and medial oblique views of the 3D-humerus geometry are presented in Figure 5.

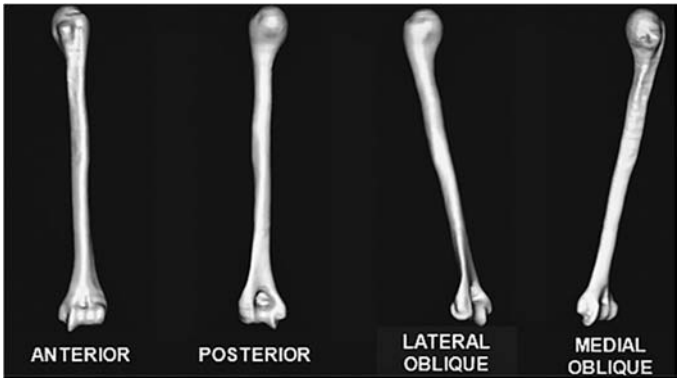

Figure 5. 3D-humerus geometry developed from the Visible Human Project image dataset.

Reference Humerus Model

Physical Model, H-VHP

The layers of the physical model were identical to the source 3D-computational geometry, and were comprised of the *cortex and cancellous layers* and a *medullary canal*. The *cortex layer* was the outer volume between the cortex mold and the core mold. The *cancellous layer* was the inner volume between the core mold and the mandrel. The *medullary canal* was the inner hollow cavity in the model that was open proximally and blind-ended distally, and was based upon the circular-cross-sectional tapered cylinder mandrel geometry. Anterior, posterior, lateral and medial views of the physical model, H-VHP, are presented in Figure 6.

3D-Computational Geometry of the H-VHP

The 3D-computational geometry of the H-VHP was comprised of three surfaces, and three derivative non-overlapping, contiguous volumes. The three surfaces were the outer cortical surface, the inner cortical/outer cancellous surface, and the inner cancellous surface. The three volumes were the outer cortical volume, between the outer and inner cortical surfaces, the inner cancellous volume, between inner cortical and inner cancellous surface, and the medullary canal volume, based upon the mandrel geometry. Anterior, posterior, lateral oblique and medial oblique views of the 3D-computational geometry of the H-VHP are presented in Figure 7.

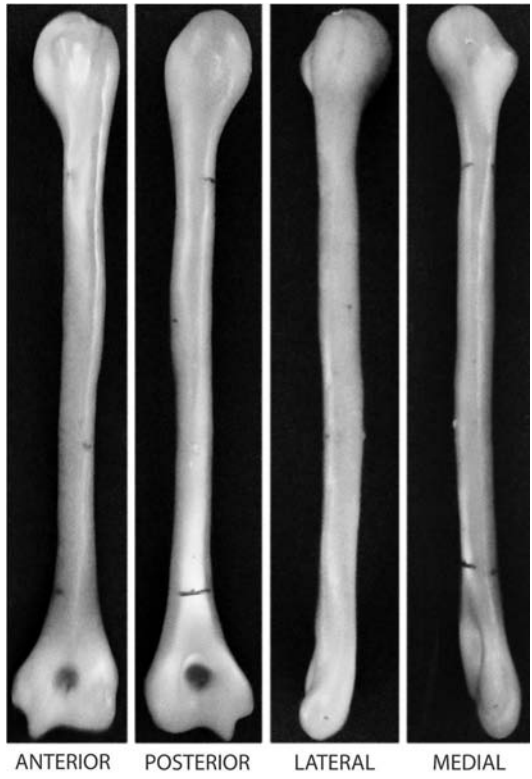

Figure 6. Physical model, H-VHP.

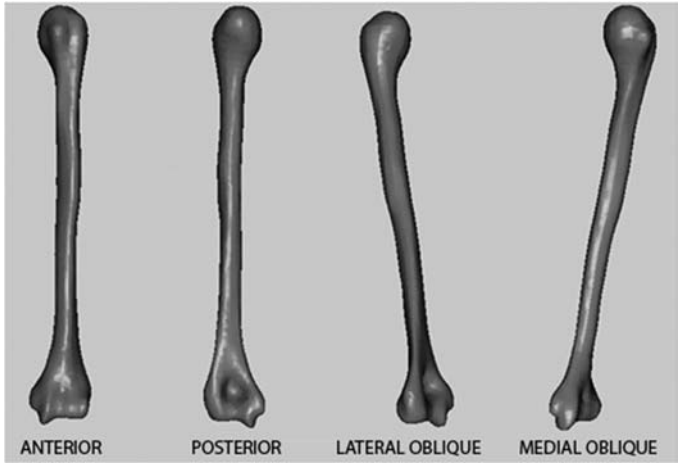

Figure 7. 3D-Computational geometry of the H-VHP.

DISCUSSION

The "Reference Humerus" model, developed based upon "definition-of-reference" criteria, from the NIH Visible Human Project, is a biomechanical tool with many applications. The model is comprised of comprising a structurally characterized physical model, H-VHP, and anatomically characterized corresponding 3D-computational geometry. Some possible clinical applications include surgical technique practice on the physical model, H-VHP, and presurgical planning with the 3D-computational geometry. Potential research applications include evaluation of trauma-fixation and arthroplasty implants using both the physical model and the geometry. The 3D-computational geometry can also be used for the development of finite element (FE) models of the humerus, which can then be used to study various musculoskeletal pathologies, including osteoporosis, bone metastasis, and OI.

Many characteristic features of OI make the evaluation of fracture risk in this pathology amenable to study by the FE method (Pathology-specific FE modeling). First, the skeletal system is the major system affected by the underlying qualitative/quantitative alteration in Type I collagen.[3] Since the FE method is already a well documented tool for studying other musculoskeletal pathologies,[25] and bones and muscles can be modeled with anatomic accuracy in FE simulations, this method is suitable for studying the skeletal manifestations in OI. Second, the clinical predisposition to fracture can be correlated with the magnitude and distribution of predefined fracture criteria parameters such as Von Mises stress and principal strain[26] that are provided by the FE solver. Third, the alteration in material properties of bone in OI, especially the longitudinal modulus, can be easily incorporated into the FE model.

Combined with bone material property and cross-sectional geometry information specific to OI, the "Reference Humerus" model, with its undeformed 3D-computational geometry, is sufficient to study the quantitative effect of altered material properties and cross-sectional geometry on fracture risk in OI. Preliminary sensitivity studies conducted by the authors indicate maximum sensitivity of fracture-risk strain criteria to the longitudinal modulus of the cortex (among material property parameters), followed by the cortical thickness and the cortical cross-sectional area (among cross-sectional geometry parameters).

Additional OI population patient-specific inputs to the pathology-specific FE model developed from the "Reference Humerus" model (Patient-specific FE modeling) can guide management of individual OI patients. The two main inputs include deformity and (kinetic and kinematic) motion analysis data. Patient-specific humeral geometry of the deformity can be obtained non-invasively using radiographic methods. These methods could involve low-radiation single-plane (plane-of-maximum-deformity) or two-plane (orthogonal) digital X-rays or, less likely, given the radiation concerns in weakened bone, higher-radiation CT scans. The 2D-geometric information can then be used to alter the "Reference Humerus" model 3D-computational geometry[27] to closely simulate patient-specific humerus geometry (OI patient-specific "Reference Humerus" FE model).

Patient-specific motion analysis data can be obtained from task-specific clinical trials, such as for Loftstrand crutch-aided ambulation. This data can then be incorporated into the OI patient-specific "Reference Humerus" FE model as loads and boundary conditions to develop an OI patient-specific task-specific "Reference Humerus" FE model. These models can provide quantitative output on the magnitude and distribution of strains in the humerus model specific to the task, which could then be used to guide individualized rehabilitation of patients.

An additional input that can increase the sophistication of the FE model for Loftstrand crutch-aided ambulation is the electromyography (EMG) data of shoulder and elbow muscles that attach on the humerus and are involved in this task. The important muscles are the Biceps for flexion, Triceps for extension, Deltoid for abduction, and Pectoralis major and Latissmus dorsi for adduction.[28] The EMG data can be used to derive muscle force magnitude[29] using muscle-modeling software.[30] This information on magnitude can be combined with task-specific line(s) of muscle action data in extant literature[31] to model EMG-based muscle action as force vectors. Individual muscle force vectors can then be applied as distributed vector loads at the respective muscle attachments on the "Reference Humerus" model 3D-computational geometry to include the effect of the major muscles in determining humerus fracture risk in OI.

While accurate mapping of the muscle attachments on to the "Reference Humerus" model 3D-computational geometry is a work in progress, the available image data from the same-source complete musculoskeletal NIH Visible Human Project image dataset will ensure accuracy. Future design

work on the "Reference Humerus" model includes development of shoulder and elbow FE models. While the utility of this tool by our research group is focused on OI, the availability of this tool to the research community for studying humerus involvement in trauma/musculoskeletal pathology is also planned. Ultimately, it is hoped that this tool will contribute to the current initiative towards standardization and establishment of worldwide data repositories.

ABBREVIATIONS AND SPECIFIC TERMINOLOGY

FE	Finite element
H-VHP	Physical model of the humerus derived from the 3D humerus geometry of the Visible Human Project
NIH VHP	National Institutes of Health Visible Human Project
OI	Osteogenesis imperfecta
Reference-Humerus	H-VHP and its 3D-Computational Geometry
3D-Humerus Geometry	Humerus geometry derived from the NIH VHP
3D-Computational Geometry	Computational geometry derived from the physical model, H-VHP

REFERENCES

1. King JD, Bobechko WP. Osteogenesis Imperfecta: an orthopaedic description and surgical review. *J Bone Joint Surg Br.* 1971;53-B(1):72-89.
2. Falvo KA, Root L, Bullough PG. Osteogenesis Imperfecta: clinical evaluation and management. *J Bone Joint Surg Am.* 1974; 56(4):783-793.
3. Sillence DO, Senn A, Danks DM. *Genetic heterogeneity in Osteogenesis Imperfecta. J Med Genet.* 1979;16:101-116.
4. Wekre LL, Eriksen EF, Falch JA. Bone mass, bone markers, and prevalence of fractures in adults with Osteogenesis Imperfecta. *Arch Osteoporos.* 2011;6(1-2):31-38.
5. Zionts LE, Nash JP, Rude R, Ross T, Stott NS. Bone mineral density in children with mild Osteogenesis Imperfecta. *J Bone Joint Surg Br.* 1995;77(1):143-147.
6. Fan Z, Smith PA, Harris GF, Rauch F, Bajorunaite R. Comparison of nanoindentation measurements between Osteogenesis Imperfecta Type III and Type IV and between different anatomic locations (femur/tibia versus iliac crest). *Connect Tissue Res.* 2007;48(2):70-75.
7. Fan Z, Smith PA, Eckstein EC, Harris GF. Mechanical properties of OI type III bone tissue measured by nanoindentation. *J Biomed Mater Res A.* 2006;79(1):71-77.
8. Jones SJ, Glorieux FH, Travers R, Boyde A. The microscopic structure of bone in normal children and patients with Osteogenesis Imperfecta: a survey using backscattered electron imaging. *Calcif Tissue Int.* 1999;64(1):8-17.
9. Rauch F, Travers R, Parfitt AM, Glorieux FH. Static and dynamic bone histomorphometry in children with Osteogenesis Imperfecta. *Bone.* 2000;26(6):581-589.

10. Gatti D, Colapietro F, Fracassi E, Sartori E, Antoniazzi F, Braga V, Rossini M, Adami S. The volumetric bone density and cortical thickness in adult patients affected by Osteogenesis Imperfecta. *J Clin Densitom.* 2003;6(2):173-177.
11. Hanscom DA, Winter RB, Lutter L, Lonstein JE, Bloom BA, Bradford DS. Osteogenesis Imperfecta. Radiographic classification, natural history, and treatment of spinal deformities. *J Bone Joint Surg Am.*1992;74(4):598-616.
12. Primorac D, Rowe DW, Mottes M, Barisić I, Anticević D, Mirandola S, Gomez Lira M, Kalajzić I, Kusec V, Glorieux FH. Osteogenesis Imperfecta at the beginning of bone and joint decade. *Croat Med J.* 2001;42(4):393-415.
13. Amako M, Fassier F, Hamdy RC, Aarabi M, Montpetit K, Glorieux FH. Functional analysis of upper limb deformities in Osteogenesis Imperfecta. *J Pediatr Orthop.* 2004;24(6):689-694.
14. Slavens BA, Bhagchandani N, Wang M, Smith PA, Harris GF. An upper extremity inverse dynamics model for pediatric Lofstrand crutch-assisted gait. *J Biomech.* 2011;44(11):2162-2167.
15. Sawbones Worldwide website. http://www.sawbones.com. Accessed February 19, 2012.
16. Sangiorgio SN, Ebramzadeh E, Longjohn DB, Dorr LD. Effects of dorsal flanges on fixation of a cemented total hip replacement femoral stem. *J Bone Joint Surg Am*. 2004;86-A(4):813-820.
17. Peindl RD, Zura RD, Vincent A, Coley ER, Bosse MJ, Sims SH. Unstable proximal extraarticular tibia fractures: a biomechanical evaluation of four methods of fixation. *J Orthop Trauma.* 2004;18(8):540-545.
18. Taddei F, Martelli S, Reggiani B, Cristofolini L, Viceconti M. Finite-element modeling of bones from CT data: sensitivity to geometry and material uncertainties. *IEEE Trans Biomed Eng.* 2006;53(11):2194-2200.
19. National Institutes of Health Visible Human Project website. http://www.nlm.nih.gov/research/visible/visible_human.html. Updated Feb 19 2012. Accessed Feb 19, 2012.
20. Viceconti M, Casali M, Massari B, Cristofolini L, Bassini S, Toni A. The 'standardized femur program' proposal for a reference geometry to be used for the creation of finite element models of the femur. *J Biomech.* 1996; 29(9):1241.
21. Abramoff MD., Magelhaes PJ, Ram SJ. Image Processing with ImageJ. *Biophotonics International*. 2004; 11(7):36-42.
22. Grover P, Albert C, Wang M, Harris GF. Mechanical characterization of fourth generation composite humerus *Proceedings of the Institution of Mechanical Engineers, Part H: Journal of Engineering in Medicine.* 2011; 225(12):1169-1176.
23. Pearl ML. Proximal humeral anatomy in shoulder arthroplasty: Implications for prosthetic design and surgical technique. *J Shoulder Elbow Surg.* 2005;14(1 Suppl S):99S-104S.
24. Brownhill JR, King GJ, Johnson JA. Morphologic analysis of the distal humerus with special interest in elbow implant sizing and alignment. *J Shoulder Elbow Surg.* 2007;16(3 Suppl):S126-132.
25. Büchler P, Ramaniraka NA, Rakotomanana LR, Iannotti JP, Farron A. A finite element model of the shoulder: application to the comparison of normal and osteoarthritic joints. *Clin Biomech (Bristol, Avon).* 2002;17(9-10):630-639.
26. Nalla RK, Kinney JH,Ritchie RO. Mechanistic fracture criteria for the failure of human cortical bone *Nature Materials* 2003; 2:164–168.
27. Zheng G, Gollmer S, Schumann S, Dong X, Feilkas T, González Ballester MA. A 2D/3D correspondence building method for reconstruction of a patient-specific 3D bone surface model using point distribution models and calibrated X-ray images. *Med Image Anal.* 2009;13(6):883-899.

28. Standring S. 40th ed. *Gray's Anatomy*. Churchill-Livingstone; 2009.
29. Lawrence JH, De Luca CJ. Myoelectric signal versus force relationship in different human muscles. *J Appl Physiol.*1983; 54(6):1653-1659.
30. Delp SL, Anderson FC, Arnold AS, Loan P, Habib A, John CT, Guendelman E, Thelen DG. OpenSim: open-source software to create and analyze dynamic simulations of movement. *IEEE Trans Biomed Eng.* 2007;54(11):1940-1950.
31. Ackland DC, Pandy MG. Lines of action and stabilizing potential of the shoulder musculature. *J.Anat.*2009:215:184-197.